Efficient evaluation of nonlocal operators in density functional theory

Ying-Chih Chen,[1,*] Jing-Zhe Chen,[2,1] Vincent Michaud-Rioux,[1] Qing Shi,[1] and Hong Guo[1,3]
[1]*Center for the Physics of Materials, Department of Physics, McGill University, Montreal, Canada H3A 2T8*
[2]*Department of Physics, Shanghai University, Shanghai 200444, China*
[3]*College of Physics and Energy, Shenzhen University, Shenzhen 518060, China*

(Received 23 August 2017; published 22 February 2018)

We present a method which combines plane waves (PW) and numerical atomic orbitals (NAO) to efficiently evaluate nonlocal operators in density functional theory with periodic boundary conditions. Nonlocal operators are first expanded using PW and then transformed to NAO so that the problem of distance-truncation is avoided. The general formalism is implemented using the hybrid functional HSE06 where the nonlocal operator is the exact exchange. Comparison of electronic structures of a wide range of semiconductors to a pure PW scheme validates the accuracy of our method. Due to the locality of NAO, thus sparsity of matrix representations of the operators, the computational complexity of the method is asymptotically quadratic in the number of electrons. Finally, we apply the technique to investigate the electronic structure of the interface between a single-layer black phosphorous and the high-κ dielectric material $c-HfO_2$. We predict that the band offset between the two materials is 1.29 eV and 2.18 eV for valence and conduction band edges, respectively, and such offsets are suitable for 2D field-effect transistor applications.

DOI: 10.1103/PhysRevB.97.075139

I. INTRODUCTION

Density functional theory (DFT) [1] is one of the most powerful atomistic methods in physics, chemistry, material science, and engineering for predicting structural and electronic properties of materials. While DFT is, in principle, exact [1], its practical implementation inevitably requires a few approximations to solve realistic and practical problems. A clever and important approximation is to reduce the nonlocal exchange and correlation interaction between electrons into some local or semilocal form such that the many-body interacting problem in solids is reduced to an effective single particle problem within a mean field. In the well-known local density approximation (LDA) [2] and generalized gradient approximation (GGA)[3], the nonlocal exchange and correlation is written in terms of the electron density, which is local, and derivatives of the density. LDA/GGA have played extremely important roles in practical applications of DFT and they give acceptable results for many materials and physical quantities [4,5]. On the other hand, as perhaps the most visible issue, the local and semilocal exchange-correlation functionals systematically underestimate band gaps of semiconductors in comparison to experimental values and possess the self-interaction problem [6]. One of its direct consequences is that the band alignment at the interface of two different semiconductors, i.e., the energy difference between their valence band maximum (VBM) and conduction band minimum (CBM), is difficult to predict accurately.

Moving forward from local and semilocal exchange correlation functionals, nonlocal hybrid functionals have been developed to overcome various issues of LDA/GGA, including the band gap problem [6,7]. The main idea of a hybrid functional is to mix nonlocal exact exchange (EXX) with local/semilocal exchange-correlation functionals. EXX partially removes the self-interaction error in the Hartree potential [6]. However, the nonlocality of EXX makes its computational cost significantly higher than that of LDA/GGA. With plane wave (PW) basis, the computational scaling of EXX is $O(N^3)$ where N is proportional to the number of electrons [8]. This unfavorable scaling makes calculations extremely expensive for crystals even when the unit cell contains only a few tens of atoms, let alone a few hundred atoms. Therefore, attempts have been made to lower the scaling by transforming PW to maximally localized Wannier functions (MLWF) [9]. Here, the key is the locality of MLWF, i.e., it has a finite range in real space, which is independent of the system size. Since locality is the inherent property of other localized basis sets such as Gaussian type orbitals and numerical atomic orbitals (NAO), computational reduction of EXX should also be achievable by these localized bases.

Very briefly, a main bottleneck for calculating EXX in localized base is the calculation of electron repulsion integrals (ERIs). For a given basis set $\{\phi_i(\mathbf{r})\}$, where $i = 1,2,\cdots N$, ERI is defined by

$$\langle ij|mn\rangle = \iint \frac{\phi_i(\mathbf{r})\phi_j(\mathbf{r})\phi_m(\mathbf{r}')\phi_n(\mathbf{r}')}{|\mathbf{r}-\mathbf{r}'|} d^3\mathbf{r} d^3\mathbf{r}'. \quad (1)$$

Even though ERIs are unchanged during the self-consistent (SC) process, and thus can, in principle, be calculated only once and saved in memory, the total number of ERIs is $O(N^4)$, which becomes computationally and memorywise prohibitive when N becomes relatively large. An effective approach to handle this problem is the resolution of identity (RI) approximation [10,11], which significantly enhances the computational efficiency of ERI by introducing a separate, auxiliary basis $\{P_\mu(\mathbf{r})\}$:

$$\phi_i(\mathbf{r})\phi_j(\mathbf{r}) \equiv \sum_\mu C_{ij}^\mu P_\mu(\mathbf{r}),$$

*chenyc@physics.mcgill.ca

where C_{ij}^{μ} are the expansion coefficients. Using $\{P_\mu(\mathbf{r})\}$, the $O(N^4)$ ERIs are decomposed to a combination of $O(N^2)$ and $O(N^3)$ matrices

$$\langle ij|mn\rangle = \sum_{\mu\nu} C_{ij}^{\mu} V_{\mu\nu} C_{mn}^{\nu},$$

$$V_{\mu\nu} = \iint \frac{P_\mu(\mathbf{r}) P_\nu(\mathbf{r}')}{|\mathbf{r}-\mathbf{r}'|} d^3\mathbf{r} d^3\mathbf{r}'. \quad (2)$$

Considering sparsity, C_{ij}^{μ} and $V_{\mu\nu}$ scale as $O(N^2)$ and $O(N)$, respectively, hence are much less memory demanding. On the accuracy side, a very simple single-zeta (SZ) plus one polarization orbital basis can already yield electronic structure values within 10% of the referenced PW results for higher-level theory [12].

The practical application of RI-type approaches to simulate crystals requires an additional approximation. For crystal supercells with periodic boundary conditions (PBC), the localized basis that satisfies the Bloch theorem is

$$\psi_I(\mathbf{r}) = \frac{1}{\sqrt{L}} \sum_{\mathbf{R}} e^{i\mathbf{k}_i\cdot\mathbf{R}} \phi_i(\mathbf{r}-\mathbf{R}), \quad (3)$$

where L is a normalization constant, $\mathbf{R}$ runs over the lattice basis and all lattice vectors, the label $I \equiv (i,\mathbf{k}_i)$ is a shorthand notation of two indices $(i,\mathbf{k}_i)$, which are the index of localized basis i and a crystal momentum in the first Brillouin zone (BZ) $\mathbf{k}_i$. The use of basis Eq. (3) requires summing over all pairs of periodic images and the primary supercell, which becomes prohibitively expensive. For this and other reasons, a common assumption is that the interaction can be neglected if the distance between two atoms and/or two supercell images is larger than a cutoff [13–15]. This way, the numerically intensive computation is focused on the primary supercell and its immediate neighboring images. This "distance-truncation" is efficient when using the short-range (SR) truncated Coulomb operator [13,16,17].

Nevertheless, in general, the bare Coulomb operator and other nonlocal operators have a long coupling range and the distance-truncation approximation degrades accuracy. This difficulty, rooted in using the localized basis Eq. (3), is well addressed by the PW basis, which requires no distance-truncation due to the extended nature of the PWs. From this point of view, a combination of localized basis and PW should achieve both low computational cost and high accuracy when dealing with nonlocal operators for crystals under PBC. This idea has been widely applied in calculating the Hartree potential in crystals [18,19]. The charge density is firstly constructed in localized base and then expressed in terms of PWs by fast Fourier transform. The Poisson equation is solved in PW base and the resulting Hartree potential is free from the distance-truncation approximation. Extending this idea to compute ERI is possible [20,21], but as mentioned above, the number of ERIs scales as $O(N^4)$ and quickly becomes computationally prohibitive as the system size increases.

In this paper, we adopt the spirit of RI as well as combining PW and localized basis to formulate a general approach to determine nonlocal operators in PBC. The resulting formulation is free of the distance-truncation approximation, thus achieving high accuracy, while the computational complexity is drastically reduced. In particular, we apply the formulation with the 2006 version of the Heyd-Scuseria-Ernzerhof hybrid-functional (HSE06) [22] to a series of zinc-blende semiconductors, and accurate results of band gaps and dispersions are shown. We then apply this formulation to a semiconductor interface to properly calculate the band alignment. Another practical application of our formulation presented here can be found in Ref. [23], where dilute doped $GaSb_xN_{1-x}$ alloy with x as small as 0.175%—the supercell contains 1,152 atoms—was analyzed at the HSE06 level for band engineering in solar fuel systems. Such large problems could not be done before at the hybrid functional level on modest computational resources, owing to the lack of an efficient methodology, a void this work fills.

In the rest of the paper, we present the theoretical formulation, numerical implementation, verification, and application of the combined PW and NAO (PW-NAO) representation of nonlocal operators in PBC. The paper is organized as follows. In Sec. II, the general nonlocal operator is derived in terms of the PW-NAO. Section III presents the numerical implementation in terms of the HSE06 functional, and the method is applied to calculate electronic properties of 19 semiconductors. The computational scaling and comparisons with other methods are also discussed. In Sec. IV, the interface between a single-layer black phosphorus (sBP) and a $c-HfO_2$ surface is investigated to predict the band alignment. Finally, a conclusion and future direction are presented in Sec. V.

II. THEORETICAL FORMULATION

The theoretical formulation of a general nonlocal operator in terms of the PW-NAO basis is discussed in this section. We present a general derivation followed by the particular case of the HSE06 hybrid functional [22] in which the nonlocal operator is the SR EXX.

A. Nonlocal operators: General formulation

In a periodic atomic lattice, any nonlocal potential operator $A(\mathbf{r},\mathbf{r}')$ satisfies the discrete translation symmetry:

$$A(\mathbf{r}+\mathbf{R},\mathbf{r}'+\mathbf{R}) = A(\mathbf{r},\mathbf{r}'),$$

where $\mathbf{R}$ is a lattice vector. Fourier transforming to momentum space, this symmetry becomes

$$A(\mathbf{r},\mathbf{r}') = \sum_{\mathbf{q}} \sum_{\mathbf{G},\mathbf{G}'} e^{-i(\mathbf{q}+\mathbf{G})\cdot\mathbf{r}} A_{\mathbf{G},\mathbf{G}'}(\mathbf{q}) e^{i(\mathbf{q}+\mathbf{G}')\cdot\mathbf{r}'},$$

$$A_{\mathbf{G},\mathbf{G}'}(\mathbf{q}) = \iint e^{i(\mathbf{q}+\mathbf{G})\cdot\mathbf{r}} A(\mathbf{r},\mathbf{r}') e^{-i(\mathbf{q}+\mathbf{G}')\cdot\mathbf{r}'} d\mathbf{r} d\mathbf{r}'. \quad (4)$$

Here bold letters $(\mathbf{q},\mathbf{G},\mathbf{G}',\mathbf{r},\mathbf{r}')$ are vectors, $\mathbf{q}$ is also the crystal momentum restricted in the first BZ, $\mathbf{G}$ and $\mathbf{G}'$ are reciprocal lattice vectors. $A_{\mathbf{q}}(\mathbf{G},\mathbf{G}')$ is the Fourier coefficient of $A(\mathbf{r},\mathbf{r}')$ and the integral is performed in whole space.

Expanding $A(\mathbf{r},\mathbf{r}')$ in terms of the basis $\psi_I(\mathbf{r})$ defined in Eq. (3), the matrix element of $A_{\mathbf{G},\mathbf{G}'}(\mathbf{q})$ in Eq. (4) is $A_{IJ,MN}(\mathbf{q})$:

$$A_{IJ,MN}(\mathbf{q}) = \sum_{\mathbf{G}\mathbf{G}'} \left\{ \int \psi_I^*(\mathbf{r}) e^{i(\mathbf{q}+\mathbf{G})\cdot\mathbf{r}} \psi_J(\mathbf{r}) d\mathbf{r} \right\}^* \times A_{\mathbf{G}\mathbf{G}'}(\mathbf{q}) \times \left\{ \int \psi_M^*(\mathbf{r}') e^{i(\mathbf{q}+\mathbf{G}')\cdot\mathbf{r}'} \psi_N(\mathbf{r}') d\mathbf{r}' \right\}. \quad (5)$$

Introducing the following quantity,

$$Y_{\mathrm{AB}}(\mathbf{q}+\mathbf{G}) \equiv \int \psi_A^*(\mathbf{r}) e^{i(\mathbf{q}+\mathbf{G})\cdot\mathbf{r}} \psi_B(\mathbf{r}) d\mathbf{r}\,, \tag{6}$$

Eq. (5) is reduced to a simpler form,

$$A_{IJ,MN}(\mathbf{q}) = \sum_{\mathbf{G}\mathbf{G}'} Y_{IJ}^*(\mathbf{q}+\mathbf{G}) A_{\mathbf{G}\mathbf{G}'}(\mathbf{q}) Y_{MN}(\mathbf{q}+\mathbf{G}'). \tag{7}$$

Momentum conservation restricts $Y_{\mathrm{AB}}(\mathbf{q}+\mathbf{G})$ to be nonzero only if $\mathbf{k}_a = \mathbf{k}_b + \mathbf{q}$. Therefore, we can omit one quantum number to simplify the equation. Replacing the shorthand label $(IJMN)$ by their corresponding NAO indices and momentums, the final expressions are

$$Y_{\mathrm{ab}}(\mathbf{k}_b, \mathbf{q}+\mathbf{G}) = \int_\Omega \psi^*_{a,\mathbf{k}_b+\mathbf{q}}(\mathbf{r}) e^{i(\mathbf{q}+\mathbf{G})\cdot\mathbf{r}} \psi_{b,\mathbf{k}_b}(\mathbf{r}) d\mathbf{r}\,, \tag{8}$$

$$\begin{aligned} A_{IJ,MN}(\mathbf{q}) &= A_{ij,mn}(\mathbf{k}_j, \mathbf{q}, \mathbf{k}_n) \\ &= \sum_{\mathbf{G}\mathbf{G}'} Y_{ij}^*(\mathbf{k}_j, \mathbf{q}+\mathbf{G}) A_{\mathbf{G}\mathbf{G}'}(\mathbf{q}) Y_{mn}(\mathbf{k}_n, \mathbf{q}+\mathbf{G}')\,. \end{aligned} \tag{9}$$

Note that the range of the integral of Eq. (8) can be limited within a unit cell Ω instead of the whole space because the quantity to be integrated is periodic. From Eq. (8), the quantity $Y(\mathbf{k}, \mathbf{q}+\mathbf{G})$ can be viewed as a transformation that turns the momentum space representation $A_{\mathbf{G}\mathbf{G}'}(\mathbf{q})$ into its NAO representation $A_{ijmn}(\mathbf{k}_j, \mathbf{q}, \mathbf{k}_n)$. Following the same derivation, the inverse transformation from $A_{ijmn}(\mathbf{k}_j, \mathbf{q}, \mathbf{k}_n)$ to $A_{\mathbf{G}\mathbf{G}'}(\mathbf{q})$ can also be achieved using the Y matrix, and it is straightforward to prove

$$\begin{aligned} A_{\mathbf{G}\mathbf{G}'}(\mathbf{q}) = \sum_{ijmn} \sum_{\mathbf{k}_j, \mathbf{k}_n} & Y_{ij}(\mathbf{k}_j, \mathbf{q}+\mathbf{G}) A_{ij,mn}(\mathbf{k}_j, \mathbf{q}, \mathbf{k}_n) \\ & \times Y_{mn}^*(\mathbf{k}_n, \mathbf{q}+\mathbf{G}'). \end{aligned} \tag{10}$$

The Y matrix in Eq. (8) is the key quantity for expressing any nonlocal operator $A(\mathbf{r}, \mathbf{r}')$ in the PW-NAO basis. It has three important properties from the computation point of view. First, it decomposes the four-index matrix into two- and three-index matrices, which greatly reduces computational cost and computer memory consumption. The expansion accuracy is systematically controlled by the kinetic energy cutoff E_{cut} of the PWs. Second, the use of PWs and, thus, Y matrix, allows the interaction range of any nonlocal operator to be infinite, since the number of unit cells in Eq. (3) is not limited. The error from distance-truncation is therefore eliminated, which is very important if the nonlocal operator decays slowly in real space. Finally, the Y matrix is a sparse matrix under (I, J) indices, i.e., Y_{IJ} is nonzero only if the basis functions ψ_I, ψ_J have direct overlap.

B. Nonlocal operators: Exact exchange

Having established the general formalism of expressing any nonlocal operator $A(\mathbf{r}, \mathbf{r}')$ in terms of PW-NAO basis, in the following we reduce the formalism for a special case where $A(\mathbf{r}, \mathbf{r}')$ is the EXX potential. In particular, we consider the HSE06 hybrid-functional [22], which expresses the exchange-correlation energy E_{xc} as

$$E_{\mathrm{xc}} = E_{\mathrm{xc}}^{\mathrm{pbe}} + \tfrac{1}{4} E_x^{\mathrm{exx,sr}} - \tfrac{1}{4} E_x^{\mathrm{pbe,sr}},$$

where $E_{\mathrm{xc}}^{\mathrm{pbe}}$ is the PBE exchange-correlation energy, $E_x^{\mathrm{exx,sr}}$ is the EXX energy calculated with the SR Coulomb interaction, and $E_x^{\mathrm{pbe,sr}}$ is the SR PBE exchange energy calculated by rescaling the exchange hole with a SR Coulomb screening factor. For more details of the HSE06 hybrid functional, we refer interested readers to the original article in Ref. [22].

The real-space expression of the SR EXX potential [22] is (collinear spin assumed)

$$V_{\mathrm{exx,sr}}^{\sigma}(\mathbf{r}, \mathbf{r}') = -\sum_{\mathrm{occ}, \mathbf{k}'} \varphi_{\mathrm{occ}}^{\mathbf{k}\sigma}(\mathbf{r}) \frac{\mathrm{erfc}(\mu|\mathbf{r}-\mathbf{r}'|)}{|\mathbf{r}-\mathbf{r}'|} \varphi_{\mathrm{occ}}^{*,\mathbf{k}\sigma}(\mathbf{r}'), \tag{11}$$

where $\mu = 0.11\ Bohr^{-1}$ and the sum is over occupied eigenstates (OCC) of the spin channel σ and $\mathbf{k}'$-points in the BZ. The Fourier coefficient of the SR coulomb operator can be derived analytically,

$$V_{\mathbf{G}}(\mathbf{q}) = \frac{4\pi}{\Omega} \delta_{\mathbf{G}\mathbf{G}'} \frac{[1 - \exp(-|\mathbf{q}+\mathbf{G}|^2/4\mu^2)]}{|\mathbf{q}+\mathbf{G}||\mathbf{q}+\mathbf{G}'|}, \tag{12}$$

which is diagonal in reciprocal space. Using Eqs. (9) and (12) to rewrite the kernel of Eq. (11) [the part with erfc$(\cdots)$ function], expanding the eigenstates with a PBC NAO basis in Eq. (3), the EXX matrix $V_{F,ij}(\mathbf{k})$ can be expressed as

$$\begin{aligned} V_{F,ij}^{\sigma}(\mathbf{k}) &= -\sum_{mn} V_{mi,nj}(\mathbf{k}, \mathbf{q}, \mathbf{k}) D_{mn}^{\sigma}(\mathbf{k}+\mathbf{q}) \\ &= -\sum_{mn} \sum_{\mathbf{q}\mathbf{G}} Y_{mi}^*(\mathbf{k}, \mathbf{q}+\mathbf{G}) V_{\mathbf{G}}(\mathbf{q}) Y_{nj}(\mathbf{k}, \mathbf{q}+\mathbf{G}) \\ &\quad \times D_{mn}^{\sigma}(\mathbf{k}+\mathbf{q})\,, \end{aligned} \tag{13}$$

where D_{mn}^{σ} is the density matrix defined by the expansion coefficient of OCC in NAO base

$$\begin{aligned} \varphi_{\mathrm{occ}}^{\mathbf{k}\sigma}(\mathbf{r}) &= \sum_l c_l^{\mathrm{occ}}(\mathbf{k}'\sigma) \psi_{l,\mathbf{k}'}(\mathbf{r}), \\ D_{mn}^{\sigma}(\mathbf{k}') &= \sum_{\mathrm{occ}} c_m^{\mathrm{occ}}(\mathbf{k}'\sigma) c_n^{*,\mathrm{occ}}(\mathbf{k}'\sigma). \end{aligned} \tag{14}$$

In Eq. (13), the Y matrix is unchanged during the SC process thus it is calculated only once and saved in memory. With a set of given k-points, the $\mathbf{q}$ vectors are chosen to ensure that $\mathbf{k}+\mathbf{q}$ is always equal to another $\mathbf{k}$-point. All $\mathbf{q}+\mathbf{G}$ vectors with kinetic energy lower than E_{cut} are used in the Y-matrix calculation. Usually Eq. (8) is used to calculate the Y matrix, but in the case that k sampling is dense, Eq. (3) is used to rewrite $Y(\mathbf{k}, \mathbf{q}+\mathbf{G})$ in Eq. (8) as a sum of $Y(\mathbf{T}, \mathbf{q}+\mathbf{G})$ by the following:

$$\begin{aligned} Y_{ij}(\mathbf{T}, \mathbf{q}+\mathbf{G}) = \delta(\mathbf{T} - \mathbf{R}_j + \mathbf{R}_i) \sum_{\mathbf{R}_i, \mathbf{R}_j} & e^{-i\mathbf{q}\cdot\mathbf{R}_i} \\ & \times \int_\Omega \phi_i(\mathbf{r} - \mathbf{R}_i) e^{i(\mathbf{q}+\mathbf{G})\cdot\mathbf{r}} \phi_j(\mathbf{r} - \mathbf{R}_j) d\mathbf{r}\,, \end{aligned} \tag{15}$$

$$Y_{ij}(\mathbf{k}, \mathbf{q}+\mathbf{G}) = \sum_{\mathbf{T}} e^{i\mathbf{k}\cdot\mathbf{T}} Y_{ij}(\mathbf{T}, \mathbf{q}+\mathbf{G})\,. \tag{16}$$

Here, the sums over translation vectors $\mathbf{R}_i$ and $\mathbf{R}_j$ only include unit cells containing basis orbitals having a nonvanishing contribution in the primary unit cell. Equation (15) is more memory efficient since $Y(\mathbf{T})$ is sparser than $Y(\mathbf{k})$. After the Y matrix is calculated, the density-matrix D($\mathbf{k}$) is updated, followed by updating $V_F(\mathbf{k})$ according to Eq. (13), until the total energy is converged self-consistently.

After self-consistency is reached in DFT, an inverse Fourier transform is performed to obtain $V_F(\mathbf{R})$ from $V_F(\mathbf{k})$,

$$V_F^\sigma(\mathbf{R}) = \frac{1}{N_{\mathbf{k}_{sc}}} \sum_{\mathbf{k}_{sc}} \exp(-i\mathbf{k}\cdot\mathbf{R}) V_F^\sigma(\mathbf{k}_{sc}), \tag{17}$$

where $\mathbf{k}_{sc}$ is the k-point used in the SC cycle. Incidentally, if enough $\mathbf{k}_{sc}$ is sampled in the SC cycle, the resulting $V_F(\mathbf{R})$ can be used to find $V_F(\mathbf{k}_{nsc})$ at other $\mathbf{k}_{nsc}$ points which were not sampled in the SC cycle, namely

$$V_F^\sigma(\mathbf{k}_{nsc}) = \sum_{\mathbf{R}} \exp(i\mathbf{k}_{nsc}\cdot\mathbf{R}) V_F^\sigma(\mathbf{R}). \tag{18}$$

We caution that the trick of Eq. (18) cannot be used if the $\mathbf{k}_{sc}$ sampling in the SC cycle is not dense enough—for instance, if only the Γ-point is sampled. A direct evaluation of Eq. (17) leads to

$$\begin{aligned} V_F^\sigma(\mathbf{R}) = {} & (-1)\times\delta(\mathbf{R}-\mathbf{R_D}-\mathbf{T}_2+\mathbf{T}_1) \\ & \times \sum_{\mathbf{T}_1,\mathbf{T}_2} \sum_{\mathbf{R_D}} \sum_{\mathbf{qG}} Y^\dagger(\mathbf{T}_1,\mathbf{q}+\mathbf{G}) D^\sigma(\mathbf{R_D}) Y(\mathbf{T}_2,\mathbf{q}+\mathbf{G}) \\ & \times \exp(i\mathbf{q}\cdot\mathbf{R_D}) V_{\mathbf{G}}(\mathbf{q}) \,, \end{aligned} \tag{19}$$

where $D(\mathbf{R_D})$ is obtained from D($\mathbf{k}$) by inverse Fourier transform. Equarion (19) is used to get $V_F(\mathbf{R})$ when k sampling is sparse/Γ only.

In summary, the key result of our theoretical formalism using PW and NAO *together* to express nonlocal operators with PBC is the Y matrix of Eq. (8). As discussed above, the properties of Y matrix allow a drastic reduction of the computational complexity. In the next section, we show that the methodology also produces results with high accuracy.

III. RESULTS AND DISCUSSION

Due to the mathematical advantages of the formalism presented above, first-principles DFT calculation at the hybrid functional level can now be carried out for supercells having large sizes, as shown in Ref. [23]. In this section, we focus on demonstrating the accuracy of the method. The error due to incompleteness of the basis set is controlled by increasing the number of both PWs and NAO, according to the need of practical applications. The computational scaling is also discussed.

A. Numerical results

Using the PW-NAO scheme, band structures of a series of zinc-blende semiconductors are calculated and compared with those obtained by PW and projector augmented wave (PAW) as implemented in the Vienna Ab initio Simulation Package (VASP) [24,25]. The PW-NAO algorithm, and the calculations presented in this paper, were done by the electronic package RESCU, which is a real-space/NAO Kohn-Sham DFT solver [26]. The core-valence interaction is represented by optimized norm-conserving Vanderbilt (ONCV) pseudopotentials (PP) with the PBE exchange-correlation functional [27]. It is known that in hybrid-functional and/or higher-level theory such as GW, including semicore shell explicitly as valence electrons is necessary for reliable results [28–34]. Therefore, whenever an element contains d electrons, the outmost shell (n shell) and the semicore shell [(n-1) shell] are always treated as valence states. Al has no d electrons, but its (n-1) shell is still included because the scattering property is improved significantly by doing so. ONCV-PPs allow more than one valence state per angular momentum channel. Here, two projectors are always used in one angular momentum channel. The quality of the PP is verified by inspecting the logarithmic derivative. PP-scattering property results are comparable to all-electron up to 8 hartree above the reference eigen energy. Spin-orbit coupling is not considered in this paper.

TABLE I. The valence electrons and the NAO basis for each element used in HSE06 calculations in this paper. SZ or DZ correspond to one or two zeta function(s) for each valence state.

Elements	Valence	SZ or DZ	Polarization	Total # of basis
B	2s2p	DZ	3d	13
C	2s2p	DZ	3d	13
N	2s2p	DZ	3d	13
Al	2s2p3s3p	SZ	3d4d	18
Si	3s3p	DZ	3d	13
P	3s3p	DZ	3d	13
S	3s3p	DZ	3d	13
Zn	3s3p3d4s	SZ	4p4d4f	25
Ga	3s3p3d4s4p	SZ	4d	18
Ge	3s3p3d4s4p	SZ	4d	18
As	3s3p3d4s4p	SZ	4d	18
Se	3s3p3d4s4p	SZ	4d	18
Cd	4s4p4d5s	SZ	5p5d4f	25
In	4s4p4d5s5p	SZ	5d4f	25
Sb	4s4p4d5s5p	SZ	5d	18
Te	4s4p4d5s5p	SZ	5d	18

After proper PBE PPs are constructed, NAO is generated with PBE by either the energy-shift method or the confined scheme [19,35]. For elements without the (n-1) shell, a standard double-zeta (DZ) plus one polarization orbital basis, with an energy-shift 50 meV and a split-norm 0.2, is used [19]. For elements with two shells, the basis is generated by the following strategy. First, the cutoff radius (r_c) of the first-zeta basis is determined by a 50 meV energy shift. This parameter produces r_c around $3 \sim 6$ Bohr for the (n-1) shell, and $6 \sim 11$ Bohr for the n shell. Then a confined potential with the same r_c is applied to generate the desired NAO basis [35]. The strength of the confined potential is 0.1 hartree. In this way, the shape of the first-zeta basis is almost the same as the free-atom state while it decreases smoothly to zero near r_c. Only one zeta function is used for occupied states. One polarization orbital, with quantum number (n,l_h+1), where l_h is the highest angular momentum of the occupied states in the n shell, is generated using the same confined potential. Its r_c is equal to the basis with the longest cutoff, which is usually the (n,l_h) state. For Al, Zn, Cd, and In, additional polarization

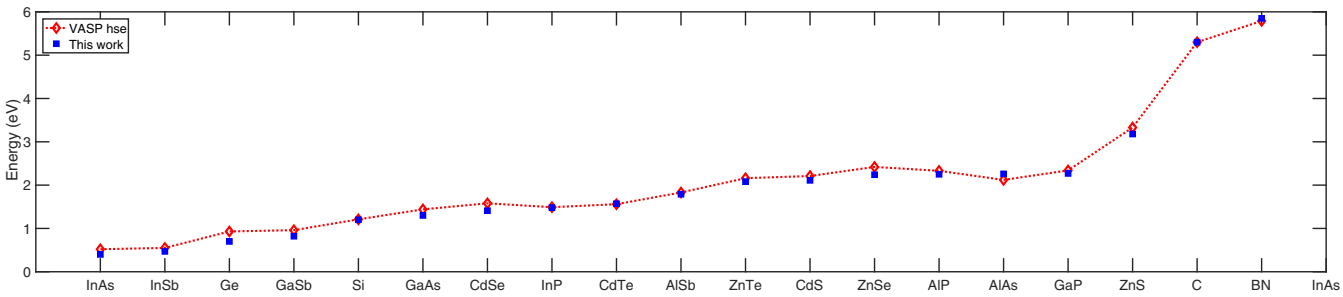

FIG. 1. Calculated HSE06 band gap of 19 semiconductors. Blue triangles are from this paper and the red dashed line with diamonds are from VASP.

orbitals are included to ensure the basis completeness. Table I summarizes the NAO basis of all elements.

In the SC DFT iteration process, $5 \times 5 \times 5$ Monkhorst-Pack k and q sampling is used for BZ integrations, except for C and BN, which use $7 \times 7 \times 7$ sampling. The E_{cut} is set to 12 hartree for the materials with Cd/Zn, and 6 hartree for the rest. The distance between two real-space points along one direction is 0.3 Bohr. The *LibXC* library is used to generate the PBE exchange-correlation part of HSE06 [36]. All results are converged with these control parameters. In VASP calculations, PBE PAW is used and d electrons are included if possible. The energy cutoff is 500 eV and the PREC is set to "accurate." The same BZ sampling is used for k and q sampling.

The lattice constant we used and the complete band structure comparison are provided in the Supplemental Material [37], where the VBM is shifted to zero to make the comparison to those obtained by VASP, and the agreement is excellent for the states near Fermi level. Here we show the band gap comparison in Fig. 1. In general, our results agree with the VASP results, with an $0.1 \sim 0.2$ eV underestimation. In practical applications of the method presented here, there are some issues to be noted. First, when a material has rather localized states (e.g., rather, flatbands), more PWs are needed. This is why a higher energy cutoff is used for materials with Cd/Zn in our calculations, to ensure the convergence of the localized d bands. Dispersive states, on the other hand, are converged with much lower E_{cut}. Second, the minor difference can be attributed to the NAO basis as only one zeta function was used for transition elements. This aspect can be systematically improved by using more zeta and polarization functions [38,39].

B. Computational complexity

It is very useful to understand the computational complexity of our method for evaluating the nonlocal operators in DFT. As shown in Eq. (13), the Y matrix and the density matrix D are needed to calculate the EXX matrix V_F. When the system is very large such as the one in Ref. [23] having 1,152 atoms, Γ-point is adequate for both k and q sampling. The Y matrix has $N_G \times N_{\text{NAO}}^2$ matrix elements where N_G is the number of PWs and N_{NAO} is the number of NAO. For each matrix element, Eq. (8) or Eq. (15) is calculated by projecting the basis and the exponential phase terms onto the real-space grid for integration. Due to the locality of NAO basis, the number of real-space grid needed is independent of the system size and the computational time for each matrix element is therefore fixed. Furthermore, if two basis functions are not directly overlapping, the corresponding Y matrix element is zero. We conclude that N_{NAO}^2 is reduced to M_1 for large systems where M_1 is the number of overlapping basis pairs. The overall computational scaling of Y matrix is actually $N_G \times M_1$.

During the SC DFT iterations, the density matrix D is updated and used to calculated V_F. Many $O(N)$ techniques are proposed, but we do not discuss them in this paper. In our calculations, a full D is used and the time complexity is $O(N_{\text{NAO}}^3)$. With a given D, the Schwarz screening is used to preselect the significant elements of V_F by the following:

$$\begin{aligned} |V_{F,ij}| &\leqslant \sum_{mn} |D_{mn}||V_{mi,nj}| \\ &\leqslant \sum_{mn} |D_{mn}||V_{mi,mi}|^{\frac{1}{2}}|V_{nj,nj}|^{\frac{1}{2}}. \end{aligned} \tag{20}$$

The number of significant elements, M_2, is proportional to the system size [14,15], M_2 should be larger than M_1. Then each significant matrix element $V_{F,ij}$ is calculated using Eq. (13). The summation of mn is limited to basis (m,i) overlap and (n,j) overlap, and is independent of the system size. Therefore, the overall computational scaling of V_F is asymptotically $N_G \times M_2$.

From the above analysis, the computational complexity appears to be more dominated by the density-matrix D calculation. Practically however, we found that the prefactor of the D calculation is rather small, and hence it becomes a bottleneck when the number of atoms is larger than several thousands. On the other hand, the Y matrix is calculated only once. Therefore, the calculation time is actually dominated by V_F. Since the magnitude is roughly $N_{\text{NAO}}^2 \gg M_2 \sim M_1 > N_G > N_{\text{NAO}}$, the time complexity of our method turns out to be slightly larger than quadratic with respect to system size. Compared to the PW scheme whose scaling is $O(N_G^3)$, it is understandable that significant computational savings are achieved by our method, so that it is not surprising that HSE06 hybrid functional calculations can now be easily performed for over 1,000 atoms on modest computers [23].

C. Further discussion

Although our formulation is applied to HSE06, it can be used for other higher level theories such as the GW under PBC [40]. The local operators are written in NAO basis and computations benefit from the relatively small basis set. The

nonlocal operators are written in PW basis and transformed to NAO whenever necessary and vice versa, based on Eqs. (8), (9), and (10). The distance-truncation approximation is avoided and the accuracy of spatially slow-decaying operators can be guaranteed. When a basis transformation is performed, the locality of NAO makes the computation more efficient and lowers the computational complexity. These properties make our formulation a potential pathway toward large-scale, high-level, theoretical calculations. We note that if the original coulomb operator is used, its Fourier coefficient $V_{\mathbf{G}}(\mathbf{q})$ is

$$V_{\mathbf{G}}(\mathbf{q}) = \frac{4\pi}{\Omega} \frac{\delta_{\mathbf{G}\mathbf{G}'}}{|\mathbf{q}+\mathbf{G}||\mathbf{q}+\mathbf{G}'|}, \tag{21}$$

and has a divergence at $\mathbf{q}=\mathbf{G}=\mathbf{0}$. To handle the divergence, we follow the spirit of Ref. [41], and generate its value by an integral

$$V_{\mathbf{0}}(\mathbf{q}_0 \to \mathbf{0}) = \frac{4\pi}{\Omega} \int_{\mathrm{BZ}\in\mathbf{q}_0} \frac{1}{|\mathbf{q}|^2} d^3\mathbf{q}. \tag{22}$$

The integral is limited in the part of BZ near Γ-point and it's solved by Monte Carlo technique. We test this scheme by calculating the band gap of bulk silicon with PBE0 [42], which is similar to HSE06 but replaces the SR Coulomb interaction with the bare one. The band gap is 1.91 eV, consistent to the result from the PAW and full-potential method [43].

IV. APPLICATION: BAND ALIGNMENT AT SEMICONDUCTOR INTERFACE

Having demonstrated the accuracy of our method, we now show its efficiency by revealing a computationally challenging problem requiring HSE06.

Thin-film BP field-effect transistors (FETs) have shown excellent electrical properties with an on-off current ratio as large as 10^5 and a high mobility of 1000 $\mathrm{cm}^2\ \mathrm{V}^{-1}\mathrm{s}^{-1}$. A principal challenge associated with phosphorene is its environmental stability. Capping materials are needed to prevent BP from exposure to oxygen, light, and moisture [44]. In the meantime, the capping material should not alter BP's electronic structure. For example, Al_2O_3, a common gate oxide, will oxidize BP and destroy its band gap [45]. Existing calculations suggest that the property of sBP is well preserved when grown on the HfO_2 (111) surface [46]. Therefore, it is an interesting perspective that HfO_2 could serve as both the gate oxide and capping material to BP. To this end, a very important material property is how bands align at the BP/HfO_2 interface.

In this section, we apply our method to predict the electronic properties of the interface between sBP and HfO_2. Here, the HfO_2 is in the cubic crystalline phase and the (111) surface orientation is chosen. We first perform calculations for two individual systems. For Hf atom 5s, 5p, 5d, and 6s, states are treated as valence electrons, and SZ plus polarization orbitals up to f are included. The band gap of sBP is found to be 0.90eV by PBE and 1.65eV by HSE06, the band gap of HfO_2 is 3.76eV by PBE and 5.25eV by HSE06. These calculated values are consistent with previous literature [47,48], confirming the quality of the NAO basis and pseudopotentials.

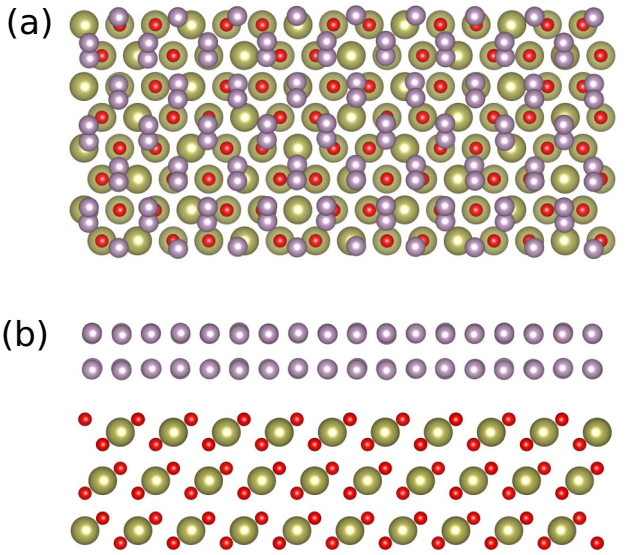

FIG. 2. (a) Top view and (b) side view of the interface structure. The purple, gold, and red balls are P atoms, Hf atoms, and O atoms, respectively.

The interface is modeled by sBP on (111) surface of a HfO_2 slab, containing 120 Hf atoms, 240 O atoms, and 108 P atoms. As shown in Fig. 2, the slab contains three layers of HfO_2 and its thickness is 7.29Å. A vacuum with thickness 14.25Å is included in the z direction. The top layer of HfO_2 and sBP are fully relaxed at the PBE level, and used in both PBE and HSE06 calculations. After the relaxation, the sBP is about 2.9Å above the HfO_2 surface. The z variation from perfect flat x-y plane of the sBP is less than 0.1Å, and is less than 0.02Å of the top HfO_2 layer. We can therefore expect the a relatively weak hybridization between the sBP and HfO_2 states.

Figure 3 shows the projected density of states (PDOS) contributed from the sBP, the top layer, and the rest of the layers of HfO_2. When the energy is 0.7eV below sBP's VBM, a hybridization between the top HfO_2 layer and sBP occurs and creates states contributed from both. Nevertheless, the band gaps after the interaction are still close to the values before the interaction. We consider the band edge of sBP and the rest of the layers of HfO_2, and show the band gap and band offset in Table II. Clearly, the band gap, as well as the band offset of the VBM (ΔVBM) and the CBM (ΔCBM), are different between PBE and HSE06 values. Especially, there's a 0.66 eV difference of ΔCBM between PBE and HSE. Since the HSE06 results suggest that HfO_2 does not change the band gap of sBP, it can serve as both the high-κ gate oxide and capping material for BP.

TABLE II. The calculated band gap and band alignment by PBE and HSE06, derived from the PDOS of the interface.

Property	PBE	HSE
sBP E_g	0.95	1.69
HfO_2 E_g	3.76	5.20
ΔCBM	1.52	2.18
ΔVBM	1.25	1.29

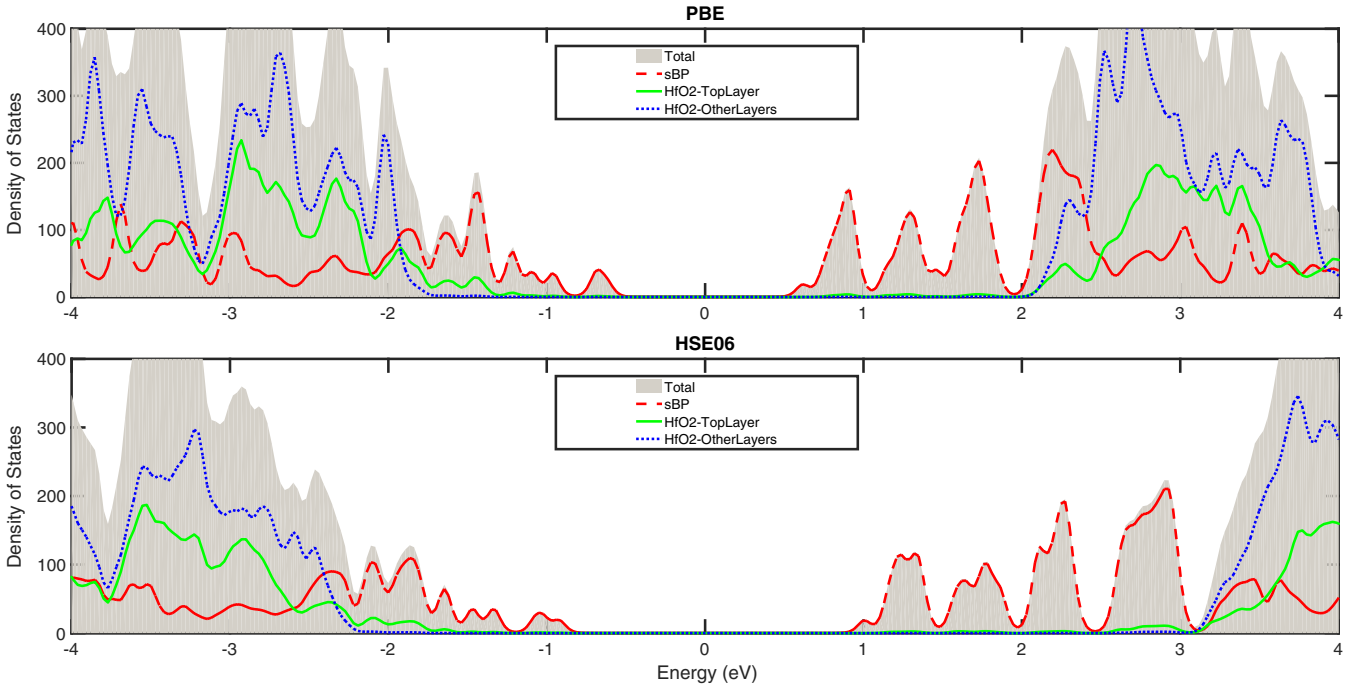

FIG. 3. Density of States by PBE and HSE.

V. CONCLUSION

In this paper, we presented a new method which combines PW and NAO to efficiently evaluate nonlocal operators with PBC. Nonlocal operators are first expanded using PW and then transformed to NAO; as such, the problem of distance truncation is avoided. The general formalism is employed to implement the hybrid functional HSE06 in which the nonlocal operator is the SR EXX interaction. Comparison to a state-of-the-art PW scheme validates the accuracy of our method. Due to the locality of NAO, thus sparsity of matrix representations of the operators, the computational complexity of our method is nearly quadratic in the number of electrons, which is the reason why very large systems can now be analyzed at the hybrid functional level [23]. In this paper, we applied our method to the SR EXX, although this general approach is applicable for all nonlocal operators under PBC.

In electronic structure calculations, hybrid functional HSE06 [22] can provide good predictions of band gaps and dispersions for many semiconductors and insulators. For pristine crystals, the primitive cell does not typically contain a large number of atoms such that the hybrid functional HSE06 can be applied despite its very heavy computational cost. There are, however, many other important problems that involve impurities, defects, roughness, interfaces, surfaces, and/or heterojunctions, for which the unit cell necessarily includes a large number of atoms to capture experimental reality. The method presented in this paper is very useful in predicting the electronic structure of these large systems. We provide an example by studying the interface between sBP and $c-HfO_2$.

ACKNOWLEDGMENTS

We gratefully acknowledge financial support of Natural Sciences and Engineering Research Council of Canada (NSERC), Fonds de recherche du Québec - Nature et technologies (FRQNT) (H.G.), and National Natural Science Foundation of China (11404206). We thank High Performance Computing of McGill University, Calcul Québec, and Compute Canada for computation facilities, which made this paper possible.

[1] W. Kohn, Nobel lecture: Electronic structure of matter-wave functions and density functionals, Rev. Mod. Phys. **71**, 1253 (1999).

[2] J. P. Perdew and Y. Wang, Accurate and simple analytic representation of the electron-gas correlation energy, Phys. Rev. B **45**, 13244 (1992).

[3] J. P. Perdew, K. Burke, and M. Ernzerhof, Generalized Gradient Approximation Made Simple, Phys. Rev. Lett. **77**, 3865 (1996).

[4] R. O. Jones and O. Gunnarsson, The density functional formalism, its applications and prospects, Rev. Mod. Phys. **61**, 689 (1989).

[5] F. Tran, R. Laskowski, P. Blaha, and K. Schwarz, Performance on molecules, surfaces, and solids of the Wu-Cohen GGA exchange-correlation energy functional, Phys. Rev. B **75**, 115131 (2007).

[6] C. Freysoldt, B. Grabowski, T. Hickel, J. Neugebauer, G. Kresse, A. Janotti, and C. G. Van de Walle, First-principles calculations for point defects in solids, Rev. Mod. Phys. **86**, 253 (2014).

[7] J. H. Skone, M. Govoni, and G. Galli, Self-consistent hybrid functional for condensed systems, Phys. Rev. B **89**, 195112 (2014).

[8] M. Marsman, J. Paier, A. Stroppa, and G. Kresse, Hybrid functionals applied to extended systems, J. Phys.: Condens. Matter **20**, 064201 (2008).

[9] X. Wu, A. Selloni, and R. Car, Order-n implementation of exact exchange in extended insulating systems, Phys. Rev. B **79**, 085102 (2009).

[10] J. L. Whitten, Coulombic potential energy integrals and approximations, J. Chem. Phys. **58**, 4496 (1973).

[11] X. Ren, P. Rinke, V. Blum, J. Wieferink, A. Tkatchenko, A. Sanfilippo, K. Reuter, and M. Scheffler, Resolution-of-identity approach to Hartree-Fock, hybrid density functionals, RPA, MP2 and GW with numeric atom-centered orbital basis functions, J. Chem. Theory Comput. **8**, 4177 (2012).

[12] H. Húbener, M. A. Pérez-Osorio, P. Ordejón, and F. Giustino, Performance of local orbital basis sets in the self-consistent Sternheimer method for dielectric matrices of extended systems, Eur. Phys. J. B **85**, 321 (2012).

[13] S. V. Levchenko, X. Ren, J. Wieferink, R. Johanni, P. Rinke, V. Blum, and M. Scheffler, Hybrid functionals for large periodic systems in an all-electron, numeric atom-centered basis framework, Comput. Phys. Commun. **192**, 60 (2015).

[14] H. Shang, Z. Li, and J. Yang, Implementation of screened hybrid density functional for periodic systems with numerical atomic orbitals: Basis function fitting and integral screening, J. Chem. Phys. **135**, 034110 (2011).

[15] C. Ochsenfeld, C. A. White, and M. Head-Gordon, Linear and sublinear scaling formation of Hartree-Fock-type exchange matrices, J. Chem. Phys. **109**, 1663 (1998).

[16] M. Guidon, F. Schiffmann, J. Hutter, and J. VandeVondele, *Ab initio* molecular dynamics using hybrid density functionals, J. Chem. Phys. **128**, 214104 (2012).

[17] M. Guidon, J. Hutter, and J. VandeVondele, Robust periodic Hartree-Fock exchange for large-scale simulations using Gaussian basis sets, J. Chem. Theory Comput. **5**, 3010 (2009).

[18] J. VandeVondele, M. Krack, F. Mohamed, M. Parrinello, T. Chassaing, and J. Hutter, QUICKSTEP: Fast and accurate density functional calculations using a mixed Gaussian and plane waves approach, Comput. Phys. Commun. **167**, 103 (2005).

[19] J. M. Soler, E. Artacho, J. D. Gale, A. García, J. Junquera, P. Ordejón, and D. Sánchez-Portal, The SIESTA method for *ab initio* order-N materials simulation, J. Phys.: Condens. Matter **14**, 2745 (2002).

[20] M. Del Ben, J. Hutter, and J. VandeVondele, Second-order Møller-Plesset perturbation theory in the condensed phase: An efficient and massively parallel gaussian and plane waves approach, New J. Phys. **14**, 053020 (2012).

[21] H. Shang, Z. Li, and J. Yang, Implementation of exact exchange with numerical atomic orbitals, J. Phys. Chem. A **114**, 1039 (2010).

[22] J. Heyd, G. E. Scuseria, and M. Ernzerhof, Erratum: hybrid functionals based on a screened coulomb potential, J. Chem. Phys. **118**, 8207 (2003); **124**, 219906 (2006).

[23] Q. Shi, Y.-C. Chen, F. A. Chowdhury, Z. Mi, V. Michaud-Rioux, and H. Guo, Band engineering of GaSbN alloy for solar fuel applications, Phys. Rev. Mater. **1**, 034602 (2017).

[24] G. Kresse and J. Furthmüller, Efficient iterative schemes for *ab initio* total-energy calculations using a plane-wave basis set, Phys. Rev. B **54**, 11169 (1996).

[25] G. Kresse and D. Joubert, From ultrasoft pseudopotentials to the projector augmented-wave method, Phys. Rev. B **59**, 1758 (1999).

[26] V. Michaud-Rioux, L. Zhang, and H. Guo, Rescu: A real space electronic structure method, J. Comput. Phys. **307**, 593 (2016).

[27] D. R. Hamann, Optimized norm-conserving vanderbilt pseudopotentials, Phys. Rev. B **88**, 085117 (2013).

[28] A. Qteish, A. I. Al-Sharif, M. Fuchs, M. Scheffler, S. Boeck, and J. Neugebauer, Role of semicore states in the electronic structure of group-iii nitrides: An exact-exchange study, Phys. Rev. B **72**, 155317 (2005).

[29] E. Engel, Relevance of semi-core-valence interaction for exact exchange calculations for group iva, iiia-va, and iib-via semiconductors, Int. J. Quantum Chem. **116**, 867 (2016).

[30] M. Städele, M. Moukara, J. A. Majewski, P. Vogl, and A. Görling, Exact exchange kohn-sham formalism applied to semiconductors, Phys. Rev. B **59**, 10031 (1999).

[31] B. Lee, L.-W. Wang, and A. Canning, Effects of d-electrons in pseudopotential screened-exchange density functional calculations, J. Appl. Phys. **103**, 113713 (2008).

[32] S. Sharma, J. K. Dewhurst, and C. Ambrosch-Draxl, All-Electron Exact Exchange Treatment of Semiconductors: Effect of Core-Valence Interaction on Band-Gap and D-Band Position, Phys. Rev. Lett. **95**, 136402 (2005).

[33] W. Chen and A. Pasquarello, Band-edge positions in gw: Effects of starting point and self-consistency, Phys. Rev. B **90**, 165133 (2014).

[34] W. Chen and A. Pasquarello, Band-edge levels in semiconductors and insulators: Hybrid density functional theory versus many-body perturbation theory, Phys. Rev. B **86**, 035134 (2012).

[35] J. Junquera, Ó. Paz, D. Sánchez-Portal, and E. Artacho, Numerical atomic orbitals for linear-scaling calculations, Phys. Rev. B **64**, 235111 (2001).

[36] M. A. L. Marques, M. J. T. Oliveira, and T. Burnus, Libxc: A library of exchange and correlation functionals for density functional theory, Comput. Phys. Commun. **183**, 2272 (2012).

[37] See Supplemental Material at http://link.aps.org/supplemental/10.1103/PhysRevB.97.075139 for the complete band structure comparison.

[38] F. Corsetti, M. V. Fernandez-Serra, J. M. Soler, and E. Artacho, Optimal finite-range atomic basis sets for liquid water and ice, J. Phys.: Condens. Matter **25**, 435504 (2013).

[39] V. Blum, R. Gehrke, F. Hanke, P. Havu, V. Havu, X. Ren, K. Reuter, and M. Scheffler, *Ab initio* molecular simulations with numeric atom-centered orbitals, Comput. Phys. Commun. **180**, 2175 (2009).

[40] J. Deslippe, G. Samsonidze, D. A. Strubbe, M. Jain, M. L. Cohen, and S. G. Louie, BerkeleyGW: A massively parallel computer package for the calculation of the quasiparticle and optical properties of materials and nanostructures, Comput. Phys. Commun. **183**, 1269 (2012).

[41] O. Pulci, G. Onida, and R. Del Sole, *Ab Initio* Calculation of Self-Energy Effects on Optical Properties of GaAs(110), Phys. Rev. Lett. **81**, 5374 (1998).

[42] J. P. Perdew, M. Ernzerhof, and K. Burke, Rationale for mixing exact exchange with density functional approximations, J. Chem. Phys. **105**, 9982 (1996).

[43] M. Betzinger, C. Friedrich, and S. Blügel, Hybrid functionals within the all-electron FLAPW method: Implementation and applications of PBE0, Phys. Rev. B **81**, 195117 (2010).

[44] M. Chhowalla, D. Jena, and H. Zhang, Two-dimensional semiconductors for transistors, Nat. Rev. Mater. **1**, 16052 (2016).

[45] Q. Shi, H. Guo, and F. Liu, Dielectric material for monolayer black phosphorus transistors: A first-principles investigation, in *Proceedings of the International Conference on Simulation of Semiconductor Processes and Devices (SISPAD)* (IEEE, Washington, D.C., 2015), pp. 56–59.

[46] F. Liu, Q. Shi, J. Wang, and H. Guo, Device Performance Simulations of Multilayer Black Phosphorus Tunneling Transistors, Appl. Phys. Lett. **107**, 203501 (2015).

[47] D. Cakir, H. Sahin, and F. M. Peeters, Tuning of the electronic and optical properties of single-layer black phosphorus by strain, Phys. Rev. B **90**, 205421 (2014).

[48] Y.-L. Yang, X.-L. Fan, C. Liu, and R.-X. Ran, First principles study of structural and electronic properties of cubic phase of ZrO_2 and HfO_2, Phys. B (Amsterdam) **434**, 7 (2014).